

# Skin-Inspired Humidity and Pressure Sensor with a Wrinkle-on-Sponge Structure

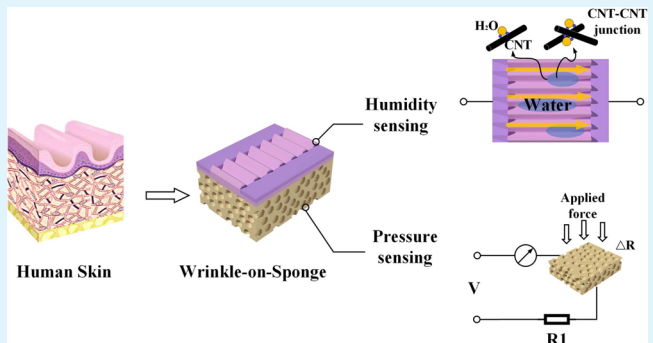
Liming Miao,<sup>†</sup> Ji Wan,<sup>†</sup> Yu Song,<sup>†</sup> Hang Guo,<sup>‡</sup> Haotian Chen,<sup>‡</sup> Xiaoliang Cheng,<sup>†</sup> and Haixia Zhang<sup>\*,†,‡</sup>

<sup>†</sup>National Key Lab of Nano/Micro Fabrication Technology and <sup>‡</sup>Academy for Advanced Interdisciplinary Studies, Peking University, Beijing 100871, China

## Supporting Information

**ABSTRACT:** Sensors with multifunctions have attracted great attention for their extensive application value, among which humidity sensing and pressure sensing are necessary to electronics undoubtedly because of the complex physical environment we live in. Inspired by the structure of skin, in this article, we design a new method to combine wrinkle structure with porous sponge structure and achieve a novel, flexible, compressible, and bifunctional sensor based on carbon nanotube–polydimethylsiloxane (CNT–PDMS) with functions of humidity sensing and pressure sensing. The performance of the humidity sensing part can be controlled by the ultraviolet and ozone (UVO) treatment time and CNT concentration, while the sensitivity of the pressure sensing part can be controlled by the CNT concentration and grinding time of sugar granules. The bifunctional sensor can easily sense approaching and touching of a hand, which shows great potential of alarming and protecting some electronics. Moreover, the bifunctional sensor can also be used in detecting human joint motions and breath conditions as a wearable and flexible health monitor.

**KEYWORDS:** skin-inspired bifunctional sensor, wrinkle-on-sponge structure, humidity and pressure sensing, robots' skin, health monitor



## 1. INTRODUCTION

With the development of smart electronics, sensors capable of detecting external changes and stimuli, such as mechanical force,<sup>1–6</sup> temperature,<sup>7–9</sup> humidity,<sup>10–12</sup> light,<sup>13</sup> and gas,<sup>14–17</sup> are becoming more and more important. Among them, humidity and pressure are two of the basic sensing items. On the one hand, humidity sensing is extremely important for electronics because high humidity environment makes them to rust easily or even causes a short circuit, which significantly affects the performance of the devices.<sup>18–20</sup> On the other hand, pressure sensing enables electronics such as robots with functions of sensing touch and force just like humans.<sup>21,22</sup> Therefore, various sensors with a single function of humidity sensing or pressure sensing were investigated and developed. Chen et al. utilized carbon nanotubes and Nafion to fabricate composite humidity sensing films which can measure low humidity sensing.<sup>23</sup> Yoo et al. realized a resistive-type relative humidity (RH) sensor based on plasma-treated multiwalled carbon nanotube/polyimide composite films and successfully explained that different carbon nanotube (CNT) concentrations resulted in different trends of resistance.<sup>24</sup> Gong et al. utilized ultrathin gold nanowires (NWs) to realize a wearable and highly sensitive pressure sensor.<sup>25</sup> All of them reported a monofunctional sensor with great performance, but there is still potential improvement in these sensors when

applied in a much more complex environment, so there remains space to study how to integrate these two types of sensing functions in one device.

To realize a bifunctional soft sensor, materials and internal structures are crucial. One-dimensional (1D) nanomaterials such as gold NWs and carbon nanotubes have unique advantages in the design and fabrication of soft electronics such as extremely large aspect ratio, which not only offers very high surface areas for electrochemical reactions but also makes them easy to form a percolation network.<sup>26</sup> Zhai et al. reported an intrinsically stretchable three-dimensional mushroom-like standing gold NW electrode to detect both glucose and strain with high performance.<sup>27</sup> He et al. utilized polyvinylidene fluoride (PVDF) and T-ZnO nanostructures to fabricate a flexible self-powered e-skin with functions of tactile perception, atmosphere detection, and self-cleaning.<sup>28</sup> Compared with Au NWs, PVDF, and T-ZnO nanostructures, CNTs, which also possess high conductivity but are more cost-effective, are a good candidate for fabricating bifunctional soft sensors.

Received: August 24, 2019

Accepted: September 26, 2019

Published: September 26, 2019

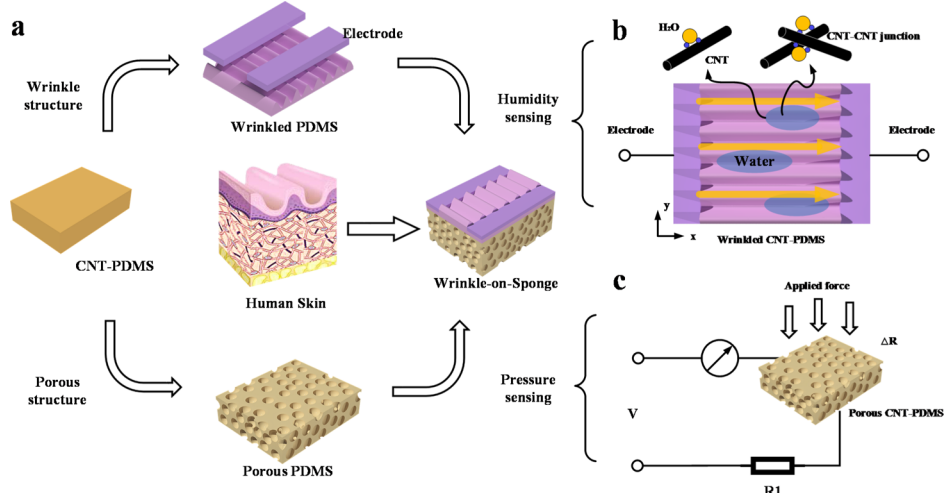


**Figure 1.** (a) Mature human skin-inspired CNT–PDMS with composite structure: wrinkle at the top and porous sponge at the bottom. (b) Illustration of a circuit of wrinkled CNT–PDMS as a humidity sensor. (c) Illustration of a circuit of porous CNT–PDMS as a pressure sensor.

As for the structural design, Nakata et al. reported a novel wearable multifunctional health care device that can detect sweat pH and skin temperature by integrating two independent sensing parts onto one piece of PET film.<sup>29</sup> Such a method is simple, but the integration is low and requires larger area for the device. Skin, as a highly integrated multifunctional “sensor” of most mammalian animals including human beings, possessing different kinds of functions such as humidity sensing, temperature, and touch sensing, has a complex and unique structure. From a physiological point of view, mammalian skin is composed of two primary layers—epidermis and dermis, where a variety of microreceptors are densely packed.<sup>30</sup> At the epidermis, the wrinkle structure increases the sensing area. Dermis has a composite matrix structure formed by collagen, elastic fibers, and extrafibrillar matrix, containing micro-mechanoreceptors that provide the function of touch sensing.<sup>31</sup>

Inspired by skin, we fabricated a bifunctional sensor with wrinkle-on-sponge structure for humidity and pressure sensing by using a carbon nanotube–polydimethylsiloxane (CNT–PDMS) composite. The bifunctional sensor shows great flexibility and compressibility. The wrinkled CNT–PDMS works as a humidity sensor and the sensitivity can be well controlled by the CNT concentration and ultraviolet and ozone (UVO) treating time. Besides, the porous CNT–PDMS sponge works as a pressure sensor and the sensitivity can also be controlled by the CNT concentration and grinding time of sugar granules. The bifunctional sensor can enable an artificial hand with the ability to sense some actions of humans like hands approaching and touching, which works as an alarm and also detects external force. Meanwhile, it can be used as a human health monitor to detect some joint motions and breath conditions while involved in some sports.

## 2. EXPERIMENTAL SECTION

**2.1. Fabrication Process for CNT–PDMS Networks.** The CNT–PDMS network was fabricated by mixing multiwalled carbon nanotubes (Boyu Co., China) with polydimethylsiloxane (Sylgard 184, Dow Corning Corporation). The length of CNTs was about 10 μm, and the quantity ratio of PDMS base solution to curing agent is 10:1. The mixing process was implemented by using a magnetic stirring apparatus for about 4 h. To improve the homogeneity of mixing CNTs with PDMS, toluene was introduced into the mixture, which makes colloidal PDMS more diluent and fluent in the stirring process.

## 2.2. Fabrication Process for Wrinkle-on-Sponge Structure.

First, the prepared CNT–PDMS mixture was poured onto the glass substrate and heated at 65 °C for 2 h, and the thickness of this CNT–PDMS layer was about 100 μm. Second, sugar granules were added into the CNT–PDMS mixture and homo-dispersed by a magnetic stirrer for 1 h. The sugar–CNT–PDMS mixture (SCPM) was then poured onto the cured CNT–PDMS layer on the glass substrate and heated at 50 °C until the curing of the SCPM to form a dual-layer structure—CNT–PDMS—at the top and SCPM at the bottom. After that, the sugar granules were reversed by immersing in a hot water bath, which led to formation of a porous structure in the SCPM with the dissolution of sugar granules. Next, we peeled off CNT–PDMS from the glass substrate, stretched it for about 30%, and carried out UVO treatment on it. Finally, the stretching strain was released, and a wrinkled CNT–PDMS structure was obtained above the porous structure. The two pieces of a copper tape with a distance of 1 mm were used as two electrodes on the wrinkled surface.

**2.3. Characterization Setup.** The UVO treatment was conducted using a commercial ultraviolet lamp (Hangzhou Yaguang lighting Co., Ltd, Zhejiang, China). The structure and morphology of the wrinkle structure and porous sponge structure were characterized by using scanning electron microscopy (SEM, Quanta 600F, FEI Co.). The optical photos of the wrinkle surface and testing water drop were characterized by using microscopy (Eclipse E200, Nikon Co.). Water contact angle measurements are recorded by the contact angle measurement system (OCA 30, Data Physics Instruments GmbH).

## 3. RESULTS AND DISCUSSION

Figure 1a shows the illustration of the sensor where the wrinkled CNT–PDMS layer is fabricated on the porous CNT–PDMS sponge, which is similar to human skin. Figure 1b shows the basic working principle of humidity sensing of wrinkled CNT–PDMS. The resistance of CNTs and the junction between CNTs change because of absorption of water molecules. In Figure 1c, the circuit of porous CNT–PDMS as a pressure sensor is shown, and the resistance is influenced by an applied force.

**3.1. Fabrication and Characterization.** The basic fabrication process can be divided into two parts: fabrication of conductive CNT–PDMS and fabrication of a wrinkle-on-sponge structure (see Figures S1 and S2 in the Supporting Information). The internal diameter, external diameter, and length of CNTs are 5–10 nm, 10–20 nm, and 10–30 μm, respectively. Such CNTs are more suitable for mixing with PDMS considering the trade-offs between the fluidity and

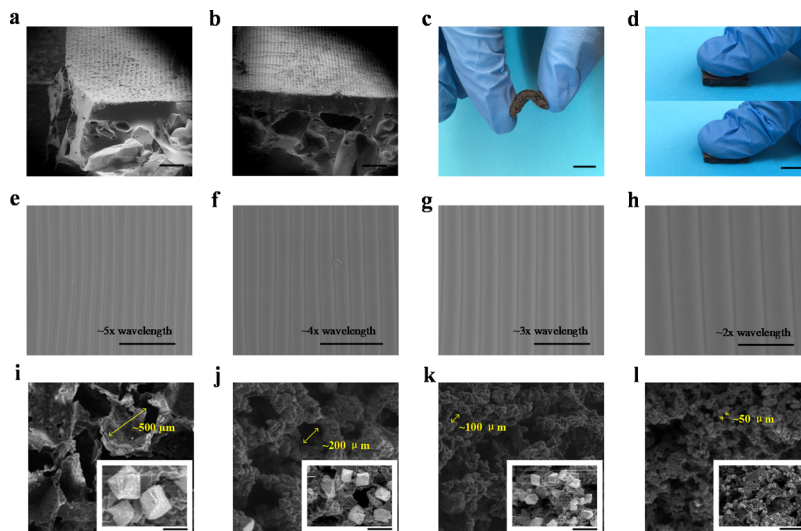


**Figure 2.** (a,b) SEM images of wrinkle-on-sponge structure. Scale bars, 500  $\mu\text{m}$ . (c,d) Optical photos show the flexibility and compressibility of the sensor with wrinkle-on-sponge structure. Scale bars, 1 cm. (e–h) SEM images of the stripe-like wrinkle structure with different wavelengths on the surface. Scale bars, 100  $\mu\text{m}$ . (i–l) SEM images of the porous sponge structure with different diameters. The white box in each image shows the sugar granules with different diameters. Scale bars, 500  $\mu\text{m}$ .

conductivity of the mixture in the experiment. The dissolution of sugar granules results in a porous structure of CNT–PDMS, which enhances the stretchability of the substrate because stretching and releasing processes are needed for wrinkle fabrication. The UVO treatment will lead to a regular stripe-like wrinkle pattern on the surface and forms a wrinkle-on-sponge structure. More experimental details can be found in **Experimental Section**.

Two types of microstructures are shown in **Figure 2**. **Figure 2a,b** shows the SEM images of the wrinkle-on-sponge structure. **Figure 2c,d** shows the optical photos of the sensor which show great flexibility and compressibility. **Figure 2e–h** shows that the wavelength of the wrinkle structure ranges from 18 to 52  $\mu\text{m}$  (the wavelength of each is about 18, 25, 35, and 52  $\mu\text{m}$ , respectively), which depends on the plasma time in wrinkle fabrication (the plasma treating time of each is 45, 60, 75, and 120 min, respectively). **Figure 2i–l** shows that the diameter of the porous sponge structure ranges from 50 to 500  $\mu\text{m}$  (the diameter of each is 500, 200, 100, and 50  $\mu\text{m}$ , respectively), which depends on the grinding time of sugar granules (the grinding time of each is 0, 1.5, 3, and 6 s, respectively).

**3.2. Wrinkled CNT–PDMS-Based Humidity Sensing.** In **Figure 3a**, it can be seen that the initial resistance of the CNT–PDMS composite polymer is a function of CNT concentration at room temperature. High CNT concentration results in the lower initial resistance of CNT–PDMS, which is demonstrated by previous works.<sup>32,33</sup> The different CNT concentrations result in two trends of humidity sensing, as shown in **Figure 3b**. To demonstrate it, all samples were treated with plasma for 60 min. When the CNT concentration is relatively low (0.3 and 1 wt % CNTs were used in the experiments), the resistance decreases with the increase of RH. In contrast, while the CNT concentration is relatively high (3 and 7 wt % CNTs were used in the experiments), the resistance increases with the increase of RH. The overall resistance of the composite wrinkled CNT–PDMS can be considered as

$$R = \sum_{\text{wrinkle}} R_{\text{CNT}} + \sum_{\text{wrinkle}} R_{\text{CNT-CNT}} \quad (1)$$

where  $R_{\text{CNT}}$  and  $R_{\text{CNT-CNT}}$  represent pure resistance of CNTs and contact resistance of CNTs, respectively. The resistance change can be attributed to these two parts.

High CNT concentration leads to a large number of CNT–CNT connections, which makes the contact resistance the main factor in resistance change. The increasing water molecules not only reduce the connections of CNTs exposed on the wrinkle surface but also make CNT–PDMS swell. Such swelling enlarges the polymer chain matrix, reducing the CNT–CNT connections in the wrinkled structure and further weakening the conductivity of contact resistance of CNTs. While the CNT concentration is low, the change of pure resistance of CNTs plays a leading role. When water molecules are absorbed by the wrinkled surface, hydronium ions can be produced as charge carriers through an ionized process when an electrostatic field is applied to the two electrodes.<sup>34,35</sup> The resistance of the hydronium ions decreases the electrical conductivity of CNTs, which behave similarly to p-type nanomaterials. As for a humidity sensor, high CNT concentration leads to less initial resistance change, which can be easily influenced by the surrounding noise. Although the curve is more linear than that of low CNT concentration, the sensitivity is lower than that of low CNT concentration in some humidity ranges, as shown in **Figure 3c**. Besides, with the increase of working temperature, the initial resistance of CNT–PDMS decreases, which influences the humidity sensing behavior (see Figure S3 in the **Supporting Information**). The sensitivity of the sample under high working temperature is relatively low, but the trend of resistance change is still the same.

Introducing a wrinkle structure onto CNT–PDMS has some unique advantages. The wrinkle structure supports a more hydrophilic and anisotropic wetting surface and enlarges the surface wetting area, which enhances the humidity sensing performance. Meanwhile, it does not change the resistance of the CNT–PDMS surface (see Figure S4 in the **Supporting Information**).

In **Figure 3d**, it can be seen that the contact angle of wrinkled surface decreases with the increase of UVO treating time. Meanwhile, the wavelength of stripe-like wrinkle increases with

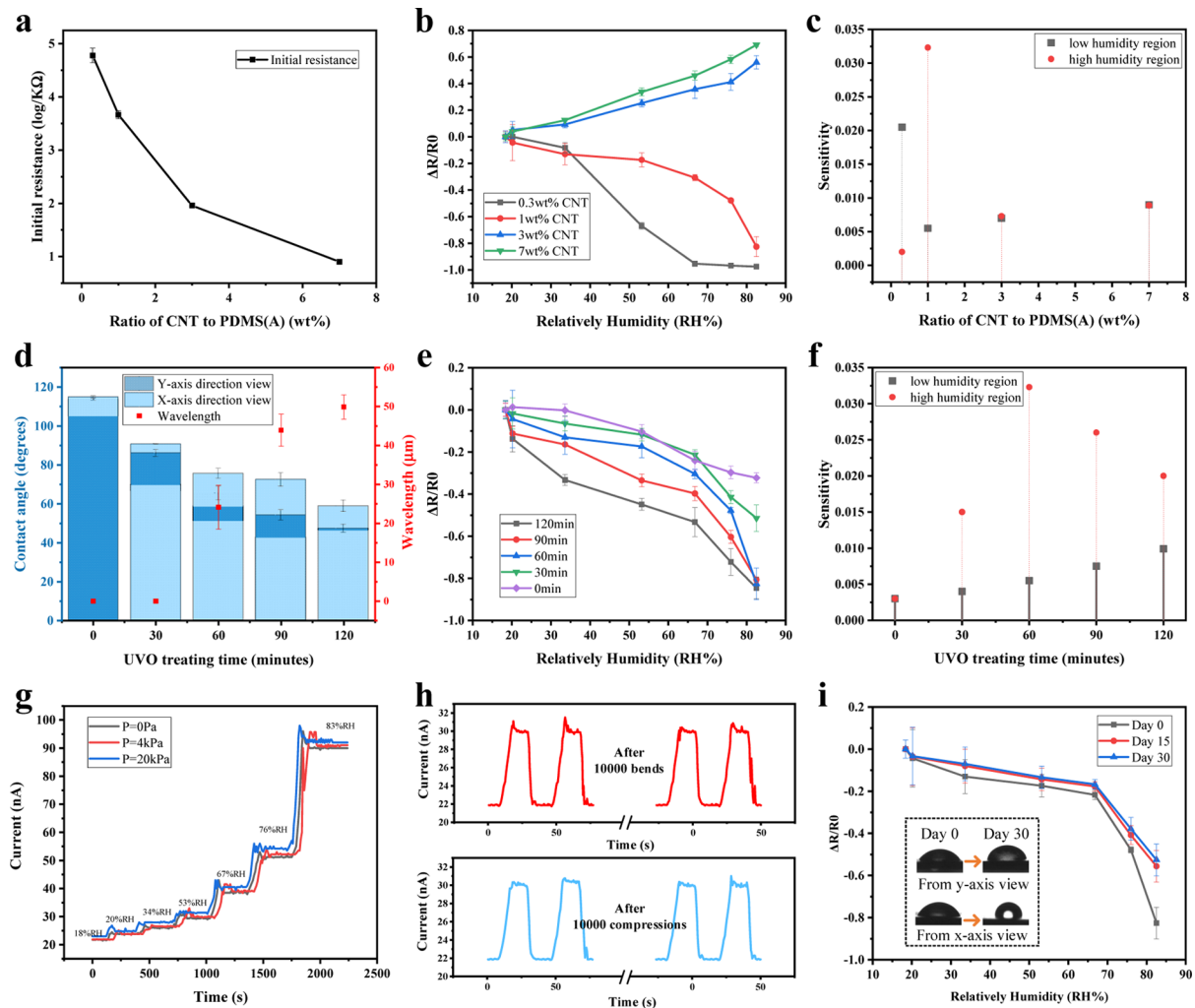


**Figure 3.** (a) Initial resistance of CNT–PDMS as a function of CNT concentration. (b) Effect of CNT concentration on RH sensing. The resistance shows different trends with different CNT concentrations. (c) Effect of CNT concentration on the sensitivity of the humidity sensor. (d) Contact angles and wavelength of stripe-like wrinkle as functions of UVO treating time. (e) Effect of UVO treating time on RH sensing. The more the UVO treating time is, the higher the degree of descent of resistance is. (f) Effect of UVO treating time on the sensitivity of the humidity sensor. (g) Real-time resistance change of the sensor with various humidity environments under different pressures. (h) Stability of the sensor after 10 000 bends and compressions. (i) Effect of time on the performance of humidity sensing and the change of contact angles.

the increase of treating time from 60 to 90 min. Especially, the regular stripe-like wrinkle cannot be obtained if the UVO treating time is less than 30 min (30 min: no wrinkle structure but the hydrophilicity is enhanced; 0 min: no wrinkle structure and original surface). To show the effect of UVO treating time, all samples have the same CNT concentration of 1%.

Figure 3e shows the function of resistance change and humidity. All samples have the same trend: resistance decreases with the increase of RH. In Figure 3f, at a low-humidity region (15–60% RH), the more the UVO treating time, the faster the resistance decreases with the increase of RH. However, at a high-humidity region (60–85% RH), samples with 60 min of UVO treating time show the highest sensitivity, which can be explained in two parts. In the first part, the UVO treating time can extremely improve the hydrophilicity of a CNT–PDMS-based surface, which enhances the absorption of water molecules, and thus, more UVO treating time shows higher sensitivity. In the second part, the wrinkle structure will influence the surface wetting properties, which is controlled by the UVO treating time.

Considering the formation process of a wrinkle structure, to a film–substrate system which contains a stiff layer and a soft layer, as the applied compress strain reaches to a certain point, the mismatch between the two layers can result in a stripe-like wrinkle structure. From mechanical analysis, the wavelength form of the wrinkle structure can be expressed as<sup>36–38</sup>

$$\lambda = 2\pi h_f \left( \frac{\bar{E}_f}{3\bar{E}_s} \right)^{1/3} \quad (2)$$

$$A = h_f \left( \frac{\varepsilon_0}{\varepsilon_c} - 1 \right)^{1/2} \quad (3)$$

where  $\bar{E}$  is the plane strain modulus given by  $\bar{E} = E/(1 - \nu^2)$ ,  $E$  is Young's modulus,  $\nu$  is the Poisson ratio, and  $h_f$  represents the stiff film thickness. The subscripts f and s denote the stiff film and soft substrate, respectively.  $\varepsilon_0$  and  $\varepsilon_c$  are the applied strain and critical strain, respectively.

With the increasing UVO treating time, the silicon oxide with high modulus on the surface also increases, which indicates that

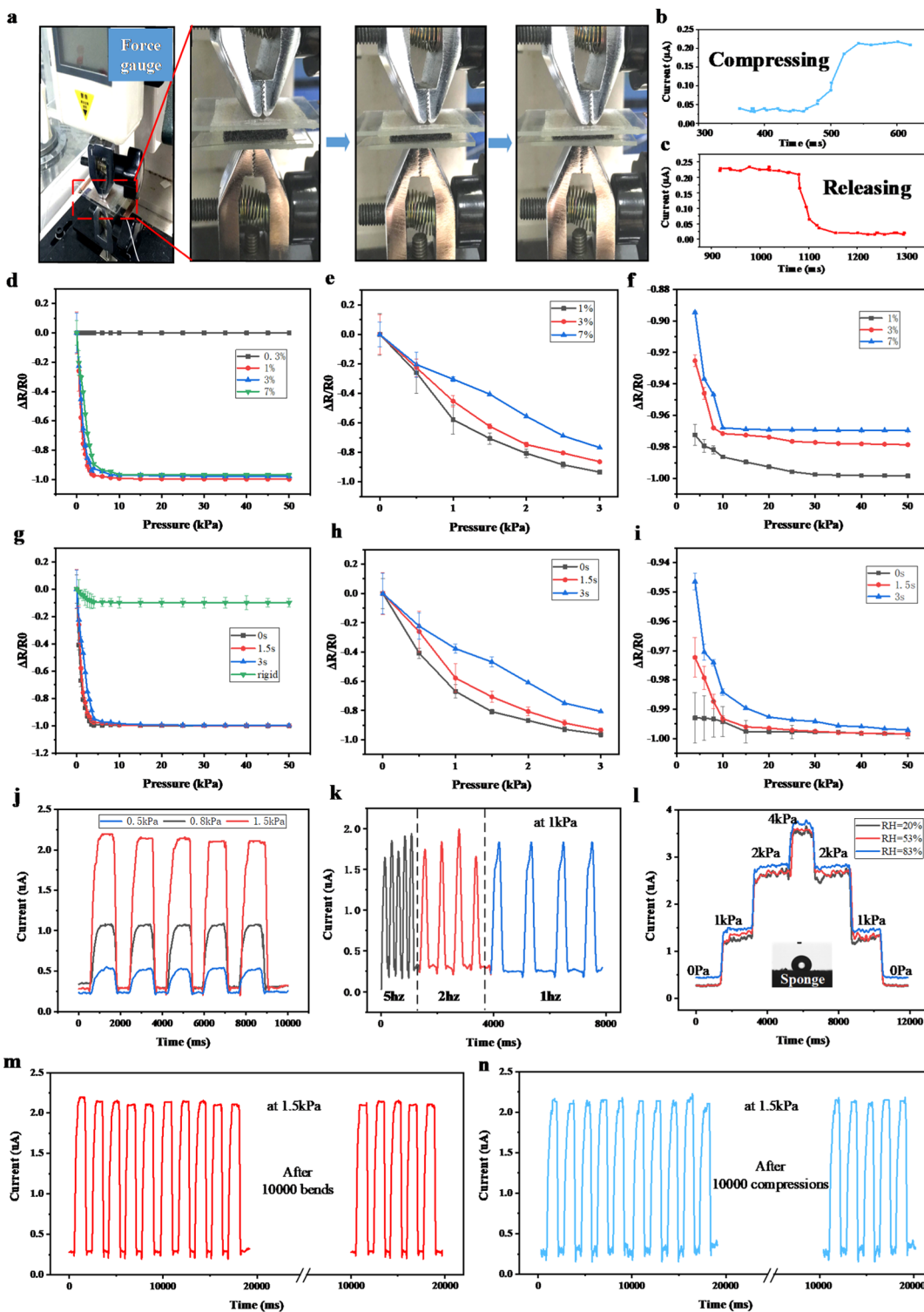


**Figure 4.** (a) Photos of experimental testing by applying normal forces. (b,c) Response performance of CNT–PDMS with porous sponge structure. (d) Effect of CNT concentration on piezoresistive performance. (e) Enlarged curves at low-pressure region. (f) Enlarged curves at high-pressure region. (g) Effect of grinding time of sugar granules on piezoresistive performance and comparison between samples with and without porous structure. (h) Enlarged curves at the low-pressure region. (i) Enlarged curves at the high-pressure region. (j) Performance of the sensor under repeated pressure. (k) Performance of the sensor with various frequencies of pressure. (l) Real-time resistance change of the sensor under different pressures with various humidity environments. (m,n) Stability of the sensor after 10 000 bends and compressions.

$h_b$ , the thickness of the stiff layer, increases and thus the wavelength of stripe-like wrinkle also increases, as shown in Figure 3d. The increasing wavelength and amplitude increase the ratio of real surface area to projected surface area, thus

enhancing the hydrophilicity of the surface. Moreover, the UVO-caused stripe-like wrinkle structure also influences the shape of the water drop while in contact with the surface. Yang et al. have demonstrated the anisotropic wettability of a liquid

droplet on a 1D stripe-like wrinkle substrate.<sup>39</sup> We also found that the droplet extended parallel to the stripe-like wrinkle (see Figure S5 in the Supporting Information) because the capillary force enhances the anisotropic diffusion of water on the wrinkle surface along the groove channels of stripe-like wrinkle.<sup>40</sup> Assisted by the stripe-like wrinkle structure, the extension of water accelerates the spread of a thin water film between the two electrodes and the absorption of water molecules through wrinkled CNT–PDMS.

Figure 3g shows the real-time resistance changes of the humidity sensing part at different humidity conditions (18, 20, 34, 53, 67, 76, and 83% RH). The sensor also stably maintains its humidity sensing part under different pressures (0 Pa, 4 kPa, and 20 kPa). Figure 3h shows the repeatability of the humidity sensing property of the sensor after 10 000 bends and compressions. Figure 3i shows that as time passes, the sensitivity of the low-humidity region decreases from 0.0055/RH % (0 day) to 0.0034/RH % (15 day) and 0.0029/RH % (30 day) and that of the high-humidity region decreases from 0.0323/RH % (0 day) to 0.0242/RH % (15 day) and 0.0229/RH % (30 day) because the hydrophilicity achieved by UVO plasma treatment is not permanent and gradually weakens by time. The contact angle of the wrinkled surface from the *x*-axis view (perpendicular to the stripe-like wrinkle) does increase sharply as the hydrophilicity weakens, while that from the *y*-axis view (parallel to the stripe-like wrinkle) increases slightly. The surface maintains the “hydrophilicity” of water in the direction parallel to stripe-like wrinkle structure because of the anisotropic diffusion between the two electrodes, for which the humidity sensing part can still work, though the performance weakens.

**3.3. Porous CNT–PDMS Sponge-Based Piezoresistive Pressure Sensing.** The basic working mechanism is shown in Figure S6a. The resistance of CNT–PDMS sponge can be simplified as

$$R = \frac{\rho l}{S} \quad (4)$$

where  $R$ ,  $\rho$ ,  $l$ , and  $S$  represent the vertical resistance, resistivity, vertical length, and cross-sectional area, respectively. The resistance change can be described as

$$\frac{\Delta R}{R} = \frac{\Delta \rho}{\rho} + \frac{\Delta l}{l} - \frac{\Delta S}{S} = \frac{\Delta l}{l} - \frac{\Delta S}{S} \quad (5)$$

Here, the resistivity of CNT–PDMS does not change under external normal pressure and  $\Delta \rho / \rho$  can be ignored. Meanwhile, the sensitivity can be calculated as

$$Se = \frac{\Delta \left( \frac{\Delta R}{R} \right)}{\Delta P} \quad (6)$$

where  $Se$  and  $P$  are the sensitivity and applied normal pressure, respectively. Considering that the curve of  $\Delta R / R$  as a function of pressure is approximately linear in the relatively low pressure and that the resistance change and external pressure are zero in the initial state, the sensitivity can be simplified as

$$Se = \frac{\left( \frac{\Delta R}{R} \right)_1 - \left( \frac{\Delta R}{R} \right)_0}{P_1 - P_0} = \frac{\left( \frac{\Delta R}{R} \right)_1}{P_1} = \frac{\frac{\Delta l_1}{l} - \frac{\Delta S_1}{S}}{P_1} \quad (7)$$

where the subscripts 1 and 0 represent the final state and initial state in the relatively low-pressure region, respectively. The hole of the sponge can easily change the vertical length and effective cross-sectional area under normal pressure for its much lower

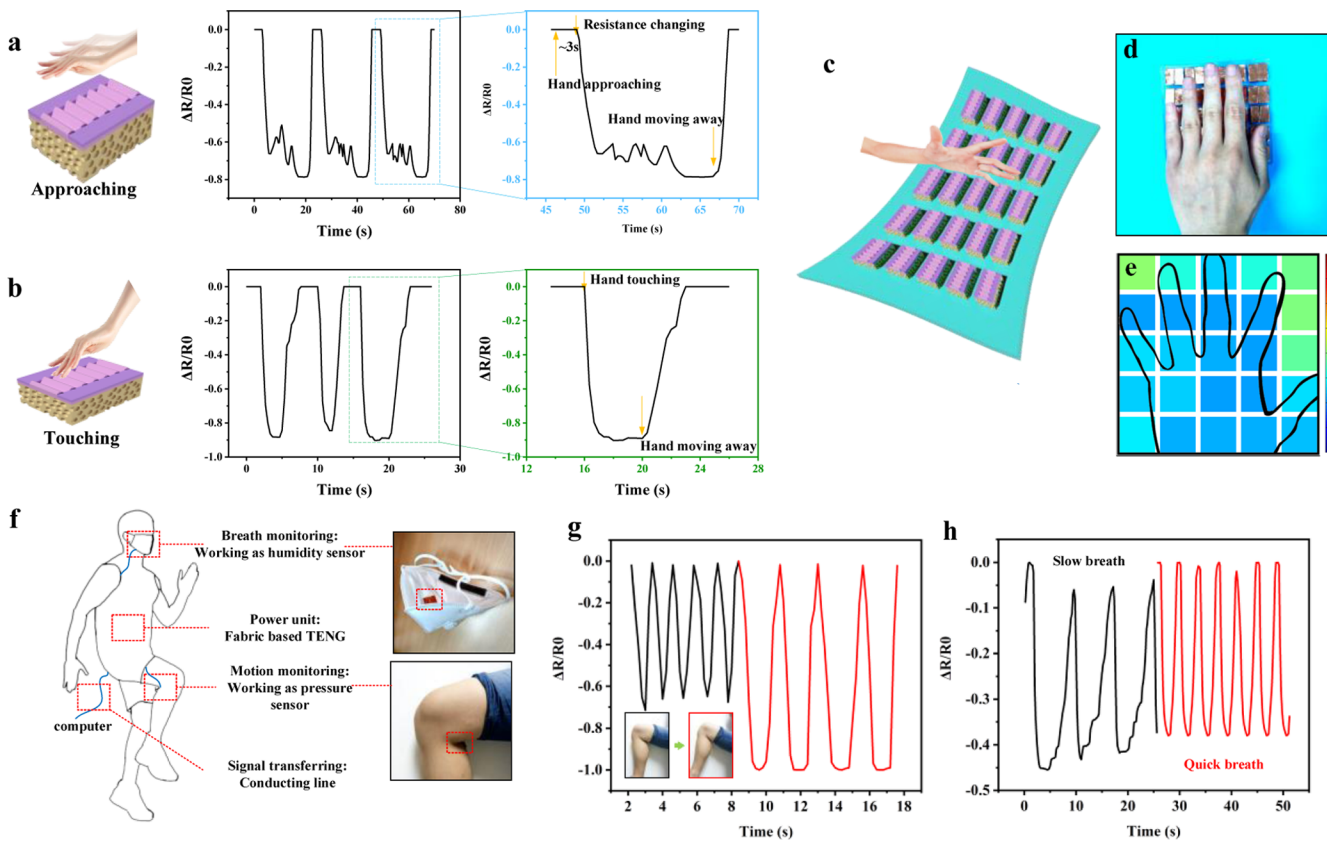
Young's modulus than the CNT–PDMS bulk without any microstructures. Therefore, the porous sponge structure is utilized to enhance the piezoresistive sensitivity of CNT–PDMS.<sup>33</sup> Figure S6c shows the exposed CNTs in the PDMS hole, and Figure S6d shows the CNT network in PDMS. Because of the low Young's modulus and high conductivity of CNTs, if the CNTs are exposed outside the PDMS hole wall which form a conductive CNT network, the resistance will quickly change with the externally applied force. The experimental testing is shown in Figure 4a, which demonstrates that the porous CNT–PDMS sponge can enhance the compressibility of the sensor. The response performance of the CNT–PDMS sponge is excellent with the rise time of 78 ms and the release time of 62.5 ms, as shown in Figure 4b,c.

Figure 4a also shows that the compressing process of the porous CNT–PDMS part can be divided into two parts: the hole wall bends first and then the CNT–PDMS bulk is compressed. When a normal force is applied onto the porous CNT–PDMS, the cavity bends and collapses, which leads to a large number of CNT connections and an increase in the conductive area of CNT–PDMS. The CNT concentration also plays an important role in piezoresistive sensing. Figure 4d shows the resistance change under different pressures. All samples were fabricated by using sugar granules which were ground for 1.5 s. Figure 4e shows that at the low-pressure region (0–3 kPa), the sensitivities of the samples with 1, 3, and 7% CNTs are 0.515, 0.438, and 0.221 kPa<sup>-1</sup>, respectively. Figure 4f shows that at the high-pressure region (more than 3 kPa), the sensitivities of the samples with 1, 3, and 7% CNTs are 0.007, 0.005, and 0.002 kPa<sup>-1</sup>, respectively. The less CNTs can easily form conductive channels when force is applied, thus improving the sensitivity. However, when the CNT concentration is as low as 0.3%, the whole CNT–PDMS does not have conductivity no matter what normal force is applied. According to the percolation theory,<sup>41</sup> 0.3% CNTs do not reach the percolation threshold, and the whole CNT conductive networks do not form in PDMS.

The size of sugar granules decides the hole size of the sponge. In the experiment, sugars are ground for about 0, 1.5, and 3 s, respectively, forming three kinds of porous CNT–PDMS sponges. The average size of holes is about 500 μm (0 s), 200 μm (1.5 s), and 100 μm (3 s), respectively. All the samples were fabricated with 1% concentration of CNTs. Figure 4g shows the different trends of resistance change with increasing pressure. The larger the size of hole is, the higher the sensitivity of the porous CNT–PDMS sponge at the low-pressure region is, just as demonstrated in Figure 4h. At the low-pressure region (0–3 kPa), the sensitivities of the samples with grinding times of 0, 1.5, and 3 s are 0.537, 0.515, and 0.311 kPa<sup>-1</sup>, respectively, because the porous CNT–PDMS sponge with large hole owns lower elastic modulus and can be easily compressed under the same normal force, which can be explained by an ideal honeycomb model. Young's modulus of the CNT–PDMS sponge in the process of bending can be considered as<sup>42</sup>

$$E = 0.22 \left( \frac{t}{b} \right)^3 E_s \quad (8)$$

where  $E_s$ ,  $t$ , and  $b$  represent Young's modulus of the bulk material, thickness of the hole wall, and length of the hole wall, respectively, hinted in Figure S6b. The larger hole possesses less thickness and larger length of the hole wall, which makes the term  $t/b$  smaller. However, at the high-pressure region, the



**Figure 5.** (a) Humidity sensing for hands approaching. The resistance decreases sharply with the hand approaching and increases with the hand moving away. (b) Pressure sensing for hands touching. The resistance changes with applying pressure quickly. (c) Schematic illustration of the sensor array. (d,e) Sensor array for sensing force. (f) Sensor fixed on a human knee joint or integrated with a mask works as a flexible health monitor. (g) Different resistance changes between normal high knee holding (black) and too high-level knee holding (red). (h) Detecting various breath states: slow breath (black) and quick breath (red).

larger hole totally collapses and Young's modulus can be observed as  $E_s$ . The compress stress concentration is exhibited at the CNT–PDMS polymer itself but not at the hole, while the smaller hole is still in the process of bending; thus, the sensitivity of the CNT–PDMS sponge with a larger hole decreases, which is less than that of porous CNT–PDMS with a smaller hole, as shown in Figure 4i. At the high-pressure region (more than 3 kPa), the sensitivities of the samples with grinding times of 0, 1.5, and 3 s are 0.003, 0.007, and  $0.02 \text{ kPa}^{-1}$ , respectively.

Figure 4j shows the performance of the sensor under various repeated pressures. The porous CNT–PDMS works stably as a pressure sensor under the repeated pressures of 0.5, 0.8, and 1.5 kPa. Figure 4k shows the response of the sensor with various frequencies of pressure. The sensor responses quickly under the pressure of 1 kPa with frequencies of 5, 2, and 1 Hz. As a bifunctional sensor system, the pressure sensor should work at different humidity environments. In Figure 4l, the real-time resistance changes of the pressure sensor can work well at RH conditions of 20, 53, and 83%. Though the wrinkled CNT–PDMS layer on the surface and the hydrophobic surface of porous CNT–PDMS well avoid the percolation of water, at the high humidity environment, the water still reduces the resistance of the porous CNT–PDMS because the water percolates through the sponge from the side wall. Figure 3h shows the repeatability of the pressure sensing property of the sensor after 10 000 bends and compressions. The samples of porous CNT–PDMS fabricated with 1% concentration of CNTs and sugar

granules by grinding for 1.5 s were tested for the results shown in Figure 4j–n.

#### 4. APPLICATION

Human skin integrates several kinds of sensors under the visible appearance, which helps us to sense almost everything in the daily life. When some organisms such as a human hand get closer to our skins, we can perceive changes in the surrounding environment, such as humidity. Furthermore, when it finally touches the skin, the microreceptors in the dermis with the function of mechanical stimuli sensing allow humans to feel the external pressure such as touching. These series of sensing are easy and common to humans. However, to any inanimate object, for example, robots, perceiving a hand approaching and touching itself is a challenging problem. The novel flexible and compressible bifunctional sensor based on CNT–PDMS with a wrinkle-on-sponge structure can solve the above problem.

In the experiment, an artificial arm of the robot was chosen as the test object and the sensor successfully helps it to achieve a similar “feeling” as an alarm device to detect sensing of a hand approaching and touching. A  $5 \times 5$  sensor array was fabricated via fixing sensors onto the ecoflex film. Because of the flexibility of the sensor itself and the adhesion of the ecoflex substrate, the sensor array can be easily affixed to the appearance of the artificial hand (see Figure S7 in the Supporting Information). When a hand approaches, the humidity near the hand improves and changes the resistance of wrinkled CNT–PDMS on the sensor's surface, playing an early warning role, as shown in

Figure 5a. When the hand touches the sensor array, the piezoresistive and porous CNT–PDMS sponge works and the resistance decreases quickly and recovers its initial value when releasing the pressure, as shown in Figure 5b. Figure 5c–e shows that the sensor array can recognize force such as a human hand, which further improves the recognition ability to the surrounding environment of robots. The surface wrinkle structure will not be destroyed even after 2000 cycles of human hand touching, which means the reliability of the sensor array is guaranteed (see Figure S8 in the Supporting Information).

As for human health monitoring, sensors are required to be flexible, weightless, or even self-powered.<sup>43,44</sup> The flexibility and weightlessness of the bifunctional sensor make itself even be easily fixed on human knee joints or integrated with a mask. Being integrated with power units such as a fabric-based triboelectric nanogenerator, conducting lines, and micro-computing chips, this sensor can work as a flexible health monitor, as shown in Figure 5f. Holding high knees is one type of the most common and popular trainings which enhances the strength of legs and joints. However, excessive high-knee training, for example, holding knees too high, may cause ligament and muscle injury. As shown in Figure 5g, the bifunctional sensor can detect how human holds his knees high via piezoresistive sensing because it receives external pressure by muscles around the knee joint. The very low resistance is a warning that knees remain too high, which may lead to injuries. In addition, the sensor integrated with a mask can be worn to detect the breath condition. According to Figure 5h, the quick breath will lead to higher frequencies of the resistance change compared to slow breath, and the curve of resistance change is more regular than that of slow breath. The quicker the breath is, the humidity changes more frequently in the relatively airtight space of the mask.

## 5. CONCLUSIONS

In summary, by mimicking the structure of skin, we have fabricated a bifunctional (humidity and pressure sensing) sensor based on CNT–PDMS with a wrinkle-on-sponge structure. CNT–PDMS is used as a conductive wrinkle substrate and materials for porous sponge. By innovatively designing the fabrication process of two structures, the wrinkle-on-sponge composite structure can be realized, which enables sensors with bifunctions: humidity sensing and pressure sensing. We find that low CNT concentration leads to a negative relationship between resistance of wrinkled CNT–PDMS and humidity, while at the relatively high CNT concentration, the resistance increases with the increase of RH. The UVO treatment controls the wrinkle structure and improves the hydrophilicity of the surface, resulting in better humidity sensing performance. As for pressure sensing, the porous sponge structure is used to enhance the sensitivity of CNT–PDMS. The CNT concentration has a great influence on the performance of pressure sensing. The lower the CNT concentration, the higher the sensitivity we obtain. The difference in the size of sugar granules also results in different sensitivities, and the sugar with the diameter of 500 μm is an optimal choice. The bifunctional sensor can enable an artificial arm with the function of sensing the approaching and touching of a hand, which guarantees normal working of electronics. Moreover, the sensor can also be used in detecting human joint motions and breath conditions just as a flexible and wearable health monitor, showing extensive application value.

## ■ ASSOCIATED CONTENT

### ■ Supporting Information

The Supporting Information is available free of charge on the ACS Publications website at DOI: 10.1021/acsami.9b13383.

Fabrication illustration of CNT–PDMS; fabrication of the multifunctional sensor based on CNT–PDMS; resistance of a thin CNT–PDMS layer before wrinkle and after wrinkle; optical photos of water wetting test; mechanism of piezoresistance and SEM images of CNTs in PDMS; sensor array covered on an artificial arm; and stability of wrinkled CNT–PDMS (PDF)

## ■ AUTHOR INFORMATION

### Corresponding Author

\*E-mail: hxzhang@pku.edu.cn.

### ORCID

Liming Miao: 0000-0003-2164-5476

Yu Song: 0000-0002-4185-2256

### Notes

The authors declare no competing financial interest.

## ■ ACKNOWLEDGMENTS

This work was supported by the National Key R&D Project from the Ministry of Science and Technology, China (2016YFA0202701 and 2016YFA0202704) and the National Natural Science Foundation of China (grant no. 61674004).

## ■ REFERENCES

- (1) Wu, H.; Su, Z.; Shi, M.; Miao, L.; Song, Y.; Chen, H.; Han, M.; Zhang, H. Self-Powered Noncontact Electronic Skin for Motion Sensing. *Adv. Funct. Mater.* **2018**, *28*, 1704641.
- (2) Chen, H.; Song, Y.; Guo, H.; Miao, L.; Chen, X.; Su, Z.; Zhang, H. Hybrid porous micro structured finger skin inspired self-powered electronic skin system for pressure sensing and sliding detection. *Nano Energy* **2018**, *51*, 496–503.
- (3) Chen, H.; Su, Z.; Song, Y.; Cheng, X.; Chen, X.; Meng, B.; Song, Z.; Chen, D.; Zhang, H. Omnidirectional bending and pressure sensor based on stretchable CNT-PU sponge. *Adv. Funct. Mater.* **2017**, *27*, 1604434.
- (4) Someya, T.; Sekitani, T.; Iba, S.; Kato, Y.; Kawaguchi, H.; Sakurai, T. A large-area, flexible pressure sensor matrix with organic field-effect transistors for artificial skin applications. *Proc. Natl. Acad. Sci.* **2004**, *101*, 9966–9970.
- (5) Tee, B. C.-K.; Chortos, A.; Dunn, R. R.; Schwartz, G.; Eason, E.; Bao, Z. Tunable flexible pressure sensors using microstructured elastomer geometries for intuitive electronics. *Adv. Funct. Mater.* **2014**, *24*, 5427–5434.
- (6) Wang, X.; Gu, Y.; Xiong, Z.; Cui, Z.; Zhang, T. Silk-molded flexible, ultrasensitive, and highly stable electronic skin for monitoring human physiological signals. *Adv. Mater.* **2014**, *26*, 1336–1342.
- (7) Kuo, C. Y.; Chan, C. L.; Gau, C.; Liu, C.-W.; Shiau, S. H.; Ting, J.-H. Nano temperature sensor using selective lateral growth of carbon nanotube between electrodes. *IEEE Trans. Nanotechnol.* **2007**, *6*, 63–69.
- (8) Shih, W.-P.; Tsao, L.-C.; Lee, C.-W.; Cheng, M.-Y.; Chang, C.; Yang, Y.-J.; Fan, K.-C. Flexible temperature sensor array based on a graphite-polydimethylsiloxane composite. *Sensors (Basel)* **2010**, *10*, 3597–3610.
- (9) Yang, J.; Wei, D.; Tang, L.; Song, X.; Luo, W.; Chu, J.; Gao, T.; Shi, H.; Du, C. Wearable temperature sensor based on graphene nanowalls. *RSC Adv.* **2015**, *5*, 25609–25615.
- (10) Borini, S.; White, R.; Wei, D.; Astley, M.; Haque, S.; Spigone, E.; Harris, N.; Kivioja, J.; Ryhänen, T. Ultrafast graphene oxide humidity sensors. *ACS Nano* **2013**, *7*, 11166–11173.

- (11) Mogera, U.; Sagade, A. A.; George, S. J.; Kulkarni, G. U. Ultrafast response humidity sensor using supramolecular nanofibre and its application in monitoring breath humidity and flow. *Sci. Rep.* **2014**, *4*, 4103.
- (12) Trung, T. Q.; Duy, L. T.; Ramasundaram, S.; Lee, N.-E. Transparent, stretchable, and rapid-response humidity sensor for body-attachable wearable electronics. *Nano Res.* **2017**, *10*, 2021–2033.
- (13) Dai, Y.; Fu, Y.; Zeng, H.; Xing, L.; Zhang, Y.; Zhan, Y.; Xue, X. A Self-Powered Brain-Linked Vision Electronic-Skin Based on Triboelectric-Photodetecting Pixel-Addressable Matrix for Visual-Image Recognition and Behavior Intervention. *Adv. Funct. Mater.* **2018**, *28*, 1800275.
- (14) Lu, G.; Ocola, L. E.; Chen, J. Reduced graphene oxide for room-temperature gas sensors. *Nanotechnology* **2009**, *20*, 445502.
- (15) Shendage, S. S.; Patil, V. L.; Vanalakar, S. A.; Patil, S. P.; Harale, N. S.; Bhosale, J. L.; Kim, J. H.; Patil, P. S. Sensitive and selective NO<sub>2</sub> gas sensor based on WO<sub>3</sub> nanoplates. *Sens. Actuators, B* **2017**, *240*, 426–433.
- (16) Fu, Y.; Zhang, M.; Dai, Y.; Zeng, H.; Sun, C.; Han, Y.; Xing, L.; Wang, S.; Xue, X.; Zhan, Y.; Zhang, Y. A self-powered brain multi-perception receptor for sensory-substitution application. *Nano Energy* **2018**, *44*, 43–52.
- (17) Xue, X.; Fu, Y.; Wang, Q.; Xing, L.; Zhang, Y. Outputting Olfactory Bionic Electric Impulse by PANI/PTFE/PANI Sandwich Nanostructures and their Application as Flexible, Smelling Electronic Skin. *Adv. Funct. Mater.* **2016**, *26*, 3128–3138.
- (18) Hübner, M.; Simion, C. E.; Tomescu-Stănoiu, A.; Pokhrel, S.; Bârsan, N.; Weimar, U. Influence of humidity on CO sensing with p-type CuO thick film gas sensors. *Sens. Actuators, B* **2011**, *153*, 347–353.
- (19) Schella, A.; Herminghaus, S.; Schröter, M. Influence of humidity on tribo-electric charging and segregation in shaken granular media. *Soft Matter* **2017**, *13*, 394–401.
- (20) Trieu, H.; Kordas, N.; okwa, W. Fully CMOS compatible capacitive differential pressure sensors with on-chip programmabilities and temperature compensation. *SENSORS*; IEEE, 2002.
- (21) Choong, C.-L.; Shim, M.-B.; Lee, B.-S.; Jeon, S.; Ko, D.-S.; Kang, T.-H.; Bae, J.; Lee, S. H.; Byun, K.-E.; Im, J.; Jeong, Y. J.; Park, C. E.; Park, J.-J.; Chung, U.-I. Highly stretchable resistive pressure sensors using a conductive elastomeric composite on a micropyramid array. *Adv. Mater.* **2014**, *26*, 3451–3458.
- (22) Zhang, J.; Shi, M.; Chen, H.; Han, M.; Song, Y.; Cheng, X.; Zhang, H. Ultra-sensitive transparent and stretchable pressure sensor with single electrode. *IEEE 29th International Conference on Micro Electro Mechanical Systems; MEMS*, 2016.
- (23) Chen, H.-W.; Wu, R.-J.; Chan, K.-H.; Sun, Y.-L.; Su, P.-G. The application of CNT/Nafion composite material to low humidity sensing measurement. *Sens. Actuators, B* **2005**, *104*, 80–84.
- (24) Yoo, K.-P.; Lim, L.-T.; Min, N.-K.; Lee, M. J.; Lee, C. J.; Park, C.-W. Novel resistive-type humidity sensor based on multiwall carbon nanotube/polyimide composite films. *Sens. Actuators, B* **2010**, *145*, 120–125.
- (25) Gong, S.; Schwalb, W.; Wang, Y.; Chen, Y.; Tang, Y.; Si, J.; Shirinzadeh, B.; Cheng, W. A wearable and highly sensitive pressure sensor with ultrathin gold nanowires. *Nat. Commun.* **2014**, *5*, 3132.
- (26) Gong, S.; Cheng, W. “One-Dimensional Nanomaterials for soft Electronics”. *Adv. Electron. Mater.* **2017**, *3*, 1600314.
- (27) Zhai, Q.; Gong, S.; Wang, Y.; Lyu, Q.; Liu, Y.; Ling, Y.; Wang, J.; Simon, G. P.; Cheng, W. Enokitake Mushroom-like Standing Gold Nanowires toward Wearable Noninvasive Bimodal Glucose and Strain Sensing. *ACS Appl. Mater. Interfaces* **2019**, *11*, 9724–9729.
- (28) He, H.; Fu, Y.; Zang, W.; Wang, Q.; Xing, L.; Zhang, Y.; Xue, X. A flexible self-powered T-ZnO/PVDF/fabric electronic-skin with multi-functions of tactile-perception, atmosphere-detection and self-clean. *Nano Energy* **2017**, *31*, 37–48.
- (29) Nakata, S.; Arie, T.; Akita, S.; Takei, K. “Wearable, Flexible, and Multifunctional Healthcare Device with an ISFET Chemical Sensor for Simultaneous Sweat pH and Skin Temperature Monitoring”. *ACS Sens.* **2017**, *2*, 443–448.
- (30) Craig, A. D. How do you feel? Interoception: the sense of the physiological condition of the body. *Nat. Rev. Neurosci.* **2002**, *3*, 655.
- (31) Breitkreutz, D.; Mirancea, N.; Nischt, R. Basement membranes in skin: unique matrix structures with diverse functions? *Histochem. Cell Biol.* **2009**, *132*, 1–10.
- (32) Chen, H.; Miao, L.; Su, Z.; Song, Y.; Han, M.; Chen, X.; Cheng, X.; Chen, D.; Zhang, H. Fingertip-inspired electronic skin based on triboelectric sliding sensing and porous piezoresistive pressure detection. *Nano Energy* **2017**, *40*, 65–72.
- (33) Jung, H.-C.; Moon, J.-H.; Baek, D.-H.; Lee, J.-H.; Choi, Y.-Y.; Hong, J.-S.; Lee, S.-H. CNT/PDMS composite flexible dry electrodes for long-term ECG monitoring. *IEEE Trans Biomed Eng.* **2012**, *59*, 1472–1479.
- (34) Tai, Y.; Lubineau, G. Human-Finger Electronics Based on Opposing Humidity-Resistance Responses in Carbon Nanofilms. *Small* **2017**, *13*, 1603486.
- (35) Tai, Y.; Bera, T. K.; Lubineau, G.; Yang, Z. Combining the converse humidity/resistance response behaviors of rGO films for flexible logic devices. *J. Mater. Chem. C* **2017**, *5*, 3848–3854.
- (36) Li, Y.; Kaynia, N.; Rudykh, S.; Boyce, M. C. Wrinkling of interfacial layers in stratified composites. *Adv. Eng. Mater.* **2013**, *15*, 921–926.
- (37) Lin, P.-C.; Yang, S. Spontaneous formation of one-dimensional ripples in transit to highly ordered two-dimensional herringbone structures through sequential and unequal biaxial mechanical stretching. *Appl. Phys. Lett.* **2007**, *90*, 241903.
- (38) Zhao, Y.; Huang, W. M.; Fu, Y. Q. Formation of micro/nano-scale wrinkling patterns atop shape memory polymers. *J. Micromech. Microeng.* **2011**, *21*, 067007.
- (39) Yang, S.; Khare, K.; Lin, P.-C. Harnessing surface wrinkle patterns in soft matter. *Adv. Funct. Mater.* **2010**, *20*, 2550–2564.
- (40) Yu, Y.; Ye, L.; Song, Y.; Guan, Y.; Zang, J. Wrinkled nitrile rubber films for stretchable and ultra-sensitive respiration sensors. *Extrem. Mech. Lett.* **2017**, *11*, 128–136.
- (41) Stauffer, D.; Aharony, A. *Introduction To Percolation Theory*; Taylor and Francis: Hoboken, NJ, USA, 2014.
- (42) Gibson, L. J.; Ashby, M. F. *Cellular Solids: Structure and Properties*; Cambridge University Press, 1999.
- (43) Fu, Y.; He, H.; Zhao, T.; Dai, Y.; Han, W.; Ma, J.; Xing, L.; Zhang, Y.; Xue, X. A Self-Powered Breath Analyzer Based on PANI/PVDF Piezo-Gas-Sensing Arrays for Potential Diagnostics Application. *Nano-Micro Lett.* **2018**, *10*, 76.
- (44) Zhong, T.; Guan, H.; Dai, Y.; He, H.; Xing, L.; Zhang, Y.; Xue, X. A self-powered flexibly-arranged gas monitoring system with evaporating T rainwater as fuel for building atmosphere big data. *Nano Energy* **2019**, *60*, 52–60.